2024 IEEE/RSJ International Conference on Intelligent Robots and Systems (IROS)
October 14-18, 2024. Abu Dhabi, UAE

Tension Feedback Control for Musculoskeletal Quadrupedal Locomotion over Uneven Terrain

Hiroaki Tanaka[1], Ojiro Matsumoto[1], Takumi Kawasetsu[1], and Koh Hosoda[2]

***Abstract*— Musculoskeletal quadruped robots driven by pneumatic artificial muscles (PAMs) have great softness. Due to the softness, the proprioceptive information of PAMs (e.g. tension) reflects the environmental information. However, how to utilize this information for stable quadrupedal gait has been rarely explored. In this work, we utilized PAM tension for stable locomotion control over uneven terrain. We newly developed a durable tension sensor and proposed tension feedback control for quadruped locomotion over uneven terrain. Our proposed controller stabilizes the trunk posture by modulating the phase of the leg. To verify the effectiveness of the proposed controller, we implement it in a simple quadrupedal model and a musculoskeletal quadruped robot driven by PAMs. Through experiments, with tension feedback, the trunk posture oscillated more stably than that without the feedback. Furthermore, over uneven terrain, the running velocity with tension feedback was higher than that without the feedback in the robot experiment. These successful results will lead to more robust musculoskeletal quadruped robots that can be employed in the real-world environment.**

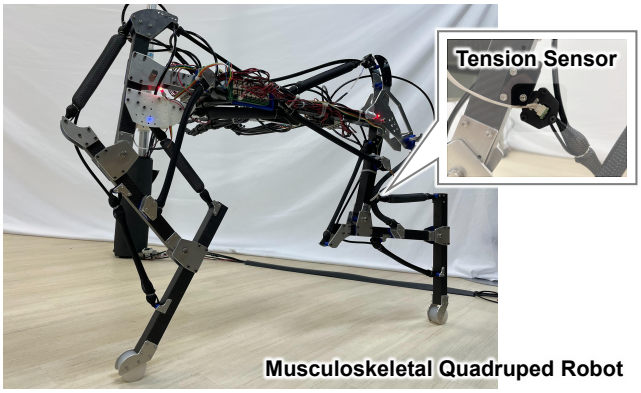

Fig. 1: Musculoskeletal quadruped robot driven by PAMs and newly developed tension sensor.

I. Introduction

Quadrupedal robots are useful tools for application in complex environments because they can choose contact points with the environment and overcome obstacles. To realize this quadrupedal locomotion, it is necessary to design adaptive gait control. Many modern quadruped robots, such as ANYmal [1] and MIT cheetah [2], compute their gait based on the robot's model acquired by mathematical modeling [3] or learning [4]. Among these robots, ANYmal first demonstrated successful walking in the challenging natural environment [5]. The key point of the study is that ANYmal utilized proprioceptive information that sensed self-movement, force, and body position. The contact force of the toe is not reliable information when the robot walks over uneven terrain because the toe does not always contact with the ground stably. Hence, ANYmal estimated the contact force from reliable proprioceptive information.

Proprioceptive information reflects both the information that drives the body and that related to contact with the environment. If the robot is soft, proprioceptive information tends to reflect the information about the contact because the robot's motion easily changes due to the contact. In the case of ANYmal, it used series elastic actuators (SEA) [6] in which a compliant spring was arranged in series with a motor. However, the control system of SEA was based on position-based control, which means that a minimum level of rigidity was required for the SEA to ensure the tracking performance of the control. This suggests that if a more soft actuator than SEA is adopted, more meaningful information about the environment can be estimated through proprioceptive information.

Pneumatic artificial muscles (PAMs) are very soft actuators [7]. PAMs modulate driving force owing to their softness, allowing the robot to adaptively contact with the environment to some extent. In addition, lightweight PAMs are useful for designing musculoskeletal quadruped robots because they do not significantly increase the leg's inertia even if redundant muscles are arranged. Utilizing these characteristics, musculoskeletal quadruped robots driven by PAMs walked [8], ran [9], and turned [10] with simple feedforward controllers.

Although many musculoskeletal quadruped robots driven by PAMs have been proposed, how to design feedback control for their locomotion over uneven terrain remains unclear mainly due to two problems. First, PAMs are difficult to control to follow a reference trajectory like model-based control. PAMs have latency and hysteresis, which degrade the model-based control performance. Second, there are no established sensors to measure proprioceptive information (e.g. tension) during the robot's locomotion. For example, a tension sensor utilizing strain gauges is easy to break due to the oscillation during the locomotion. Therefore, the previous study used the contact sensor to detect contact with the obstacles, but it was not reliable information [11].

In this work, we proposed tension feedback control for a musculoskeletal quadruped robot driven by PAMs by solving these two problems. To maintain the trunk posture even

Authors are with [1]Graduate School of Engineering Science at Osaka University, Japan, and [2] Graduate School of Engineering at Kyoto University, Japan. Corresponding Author: tanaka.hiroaki@arl.sys.es.osaka-u.ac.jp

when the robot runs over uneven terrain, the controller modulates the robot's gait by using non-linear oscillators. This non-linear oscillators calculate the phase of each leg by providing tension feedback. This control architecture does not need precise control because each PAM is only activated or deactivated based on the phase of the leg. Moreover, we newly developed a durable tension sensor based on the soft tactile sensor [12]. By using this sensor, our developed quadruped robot could measure muscle tension even when it ran over uneven terrain.

The structure of this study is as follows. In Section Ⅱ, we describe the overview of tension feedback control. In Section Ⅲ, we validate the effectiveness of the proposed control by using a simple quadrupedal model. In Section Ⅳ, we describe the robot's hardware design including a newly developed tension sensor and control. In Sections V and VI, we describe a running experiment over uneven terrain.

II. Tension Feedback Control

The gait of the quadruped robot is calculated by using a nonlinear oscillator. This nonlinear oscillator models the neural circuit called Central Pattern Generator (CPG) [13] which governs animal locomotion. The previous studies demonstrated that the legged robots could walk and run adaptively over uneven terrain by using CPG-based nonlinear oscillators [14]. However, how to utilize PAM tension for a nonlinear oscillator design has been rarely explored.

In this study, we proposed a non-linear oscillator for a musculoskeletal quadruped robot driven by PAMs. To conduct preliminary considerations, we started to consider simple bounding and pronking gaits. During these gaits, each pair of fore and hind legs can be considered as a single leg because the right and left legs move in parallel. The proposed nonlinear oscillator is formulated as follows

$$\dot{\phi}_F = \omega + \epsilon_F sin(\phi_H - \phi_F - \Delta\phi) - \sigma_F T_F cos(\phi_F), \quad (1)$$

$$\dot{\phi}_H = \omega + \epsilon_H sin(\phi_F - \phi_H + \Delta\phi) - \sigma_H T_H cos(\phi_H), \quad (2)$$

where $\phi_i \in [0, 2\pi)$ $(i = F, H)$ is the phase of the fore and hind legs, ω is the intrinsic angular velocity, ϵ_i and σ_i $(i = F, H)$ are the design parameters, $\Delta\phi$ is the phase difference between ϕ_F and ϕ_H, and T_i $(i = F, H)$ is the tension of the artificial muscles arranged in the fore and hind legs.

This model calculates the phase relationship between the fore and hind legs to maintain the trunk posture. 2nd term in Eqs. (1) and (2) means maintaining the phase difference between the front and hind legs at $\Delta\phi$ [15]. 3rd term in Eqs. (1) and (2) means that ϕ_i is modulated to pull towards $3\pi/2$ when T_i increases [16]. In our controller setting, the fore and hind legs generate pushing-off force for $\pi \leq \phi_i < 2\pi$, which means that larger T_i induces large leg extension. Considering these effects, Fig. 2 illustrates the gait adaptation mechanism over uneven terrain [14]. When the hind leg steps on an obstacle, the trunk inclines. Thus, the load is concentrated on the fore leg, and muscle tension in the fore leg's muscle increases. By providing tension feedback, as Eqs. (1) and (2), the fore leg extends more than the hind leg to maintain the trunk posture. On the other hand, when the fore leg steps on an obstacle, the hind leg extends more than the fore leg to maintain the trunk posture.

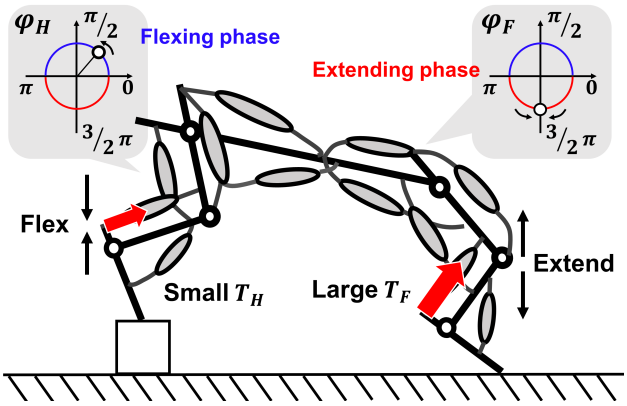

Fig. 2: Gait adaptation mechanism over uneven terrain.

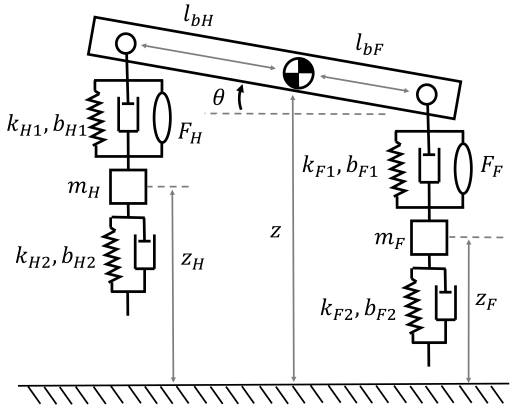

Fig. 3: Simple quadruped model.

III. Simple Model Analysis

A. Simple Quadruped Model

Before real robot experiments, we conducted numerical simulations to validate that our controller could stabilize the trunk posture. We used a simple quadruped model which consists of a trunk (mass: M, and inertia: I) and fore and hind legs (mass: m_i $(i = F, H)$) in the sagittal plane [17]. The center of gravity of the trunk is shifted $l_{bH} - l_{bF}$ forward from the center. This model focuses on the trunk posture angle θ and the vertical position of the trunk z, fore leg z_F, and hind leg z_H. It should be noted that the horizontal dynamics are ignored because we focus on how to stabilize the trunk posture by modulating the vertical extension of the fore and hind legs.

The equation of motion is given by

$$M(q)\ddot{q} + H(q, \dot{q}) + G(q) = Q, \quad (3)$$

where $q = [z, \theta, z_F, z_H]^\top$. $M(q)$, $H(q, \dot{q})$, $G(q)$, and Q represent inertia matrix, Coriolis and centrifugal forces, conservative forces, and actuator input, respectively.

TABLE I: Model parameters

Parameter	Value
M	6.0 [kg]
l_{bF}	0.2 [m]
l_{bH}	0.4 [m]
I	0.96 [kgm^2]
m_F	1.0 [kg]
m_H	1.0 [kg]
l_{F1}, l_{F2}, l_{H1}, l_{H2}	0.15 [m]
k_{F1}	8.0×10^3 [N/m]
k_{F2}	1.0×10^3 [N/m]
k_{H1}	1.0×10^4 [N/m]
k_{H2}	1.0×10^3 [N/m]
b_{F1}, b_{F2}, b_{H1}, b_{H2}	50.0 [Ns/m]
A_F	1.5×10^3
A_H	1.0×10^3
g	9.81 [m/s^2]
Δ_F, Δ_H	0.4
ω	15.7 [rad/s]
ϵ_F, ϵ_H	1.0
$\Delta\phi$	π/3 [rad]

TABLE II: Difference of maximum and minimum value of θ before/after perturbation $\Delta\theta_{max}, \Delta\theta_{min}$.

	$\Delta\theta_{max}$ [deg]	$\Delta\theta_{min}$ [deg]
$(\sigma_F, \sigma_H) = (0.3, 0.2)$	1.9443	5.5088
$(\sigma_F, \sigma_H) = (0, 0)$	3.4233	5.7697

This model has two points imitating the leg driven by PAMs: (i) Each leg has parallel k_{i1}, b_{i1} and series k_{i2}, b_{i2} elastic components with the actuation component F_i $(i = F, H)$. The natural length of the parallel and series elastic components are l_{i1} and l_{i2} $(i = F, H)$, and these series and parallel elastic components are connected through the point mass of the fore and hind legs m_i. (ii) Tension (T_i) can be measured through the series elastic components as follows

$$T_i = \begin{cases} -k_{i2}\left(z_i - l_{i2}\right) - b_{i2}\dot{z}_i & \left(z_i - l_{i2} < 0, \dot{z}_i < 0\right) \\ -k_{i2}\left(z_i - l_{i2}\right) & \left(z_i - l_{i2} < 0, \dot{z}_i \geq 0\right) \end{cases} \tag{4}$$

Note that this tension (T_i) imitates muscle tension that reflects actuation and contact force simultaneously.

This quadruped model is actuated by F_i $(i = F, H)$. In our nonlinear oscillator setting, F_i should generate pushing-off force when $\pi \leq \phi_i < 2\pi$. Therefore, we define F_i based on the privious research [18]:

$$F_i = \frac{A_i}{\sqrt{2\pi\Delta_i}} \exp\left(-\frac{\left(\phi_i - 3\pi/2\right)^2}{2\Delta_i}\right), \tag{5}$$

where A_i and Δ_i $(i = F, H)$ are design parameters.

These equations for this system are numerically integrated using the ode45 solver in MATLAB. Table I presents the model parameters for solving the equations. Although these parameters are mainly based on the developed robot explained in the next section, ω, k_{Fi}, k_{Hi}, b_{Fi}, and b_{Hi} are determined such that numerical calculations do not diverge.

B. Simulation

We validated that our CPG-based controller stabilized the trunk posture by perturbing the locomotion of the simple quadrupedal model. To perturb the locomotion, we added perturbation to the angular velocity of the posture angle $\dot{\theta}$ in the periodically stable solution. This perturbation replicates the over-tilting of the trunk and the asymmetry of tension between the fore and hind legs caused by stepping on the obstacles.

Here, we perturbated the periodically stable solution in the following step.

1) Obtain a periodically stable solution by solving the equations for 5 [s].
2) Add perturbation $\Delta\dot{\theta}$ to $\dot{\theta}$ when the trunk reaches the highest point.

When $\Delta\dot{\theta} > 0$, the perturbation causes the trunk to tilt forward. Conversely, when $\Delta\dot{\theta} < 0$, the perturbation causes

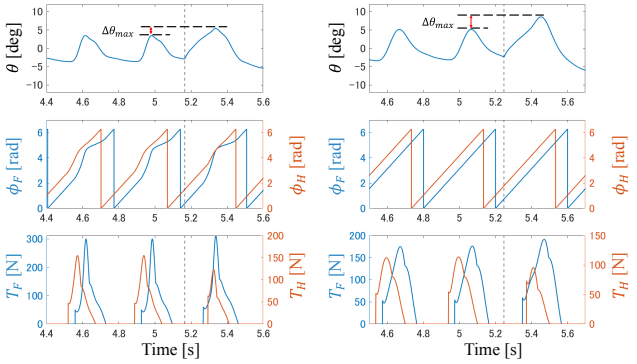

(a) With tension feedback (b) Without tension feedback

Fig. 4: Simulation result with $(\sigma_F, \sigma_H) = (0.3, 0.2)$ and without $(\sigma_F, \sigma_H) = (0, 0)$ tension feedback when $\Delta\dot{\theta} = 2.0$ [rad/s]. Phase (ϕ_F, ϕ_H), trunk posture angle (θ), and tension (T_F, T_H) are shown. Gray dashed line shows perturbing time. $\Delta\theta_{max}$ is difference in local maximum value of θ before/after perturbation.

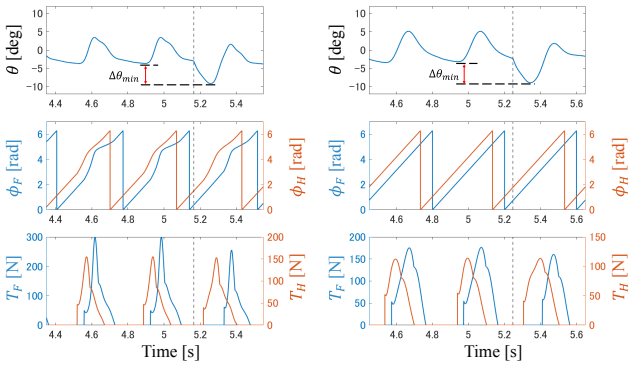

(a) With tension feedback (b) Without tension feedback

Fig. 5: Simulation result with $(\sigma_F, \sigma_H) = (0.3, 0.2)$ and without $(\sigma_F, \sigma_H) = (0, 0)$ tension feedback when $\Delta\dot{\theta} = -2.0$ [rad/s]. Phase (ϕ_F, ϕ_H), trunk posture angle (θ), and tension (T_F, T_H) are shown. Gray dashed line shows perturbing time. $\Delta\theta_{min}$ is difference in local minimum value of θ before/after perturbation.

the trunk to tilt backward. It should be noted that the perturbating condition is aligned to compare the control performance.

We validated the effectiveness of the proposed controller by comparing the cases with and without tension feedback. The results when $\Delta\dot{\theta} = 2.0$ [rad/s] are shown in Fig. 4. Both with and without tension feedback, the trunk was tilted forward after perturbation. In addition, the peak of T_F increased, and the peak of T_H decreased after the quadrupedal model was disturbed. Due to the tension feedback, the variation of T_F and T_H modulated ϕ_F and ϕ_H, such that ϕ_F was delayed. Consequently, with tension feedback, the over-tilting forward of the trunk was suppressed. In fact, the difference in the local maximum value of θ before/after perturbation ($\Delta\theta_{max}$) is smaller than that without tension feedback. From Table II, $\Delta\theta_{max}$ with tension feedback is lower than that without tension feedback.

Conversely, the results when $\Delta\dot{\theta} = -2.0$ [rad/s] are shown in Fig. 5. Both with and without tension feedback, the trunk was tilted backward after perturbation. Furthermore, the peak of T_F decreased after the quadrupedal model was perturbed. However, the over-tilting backward of the trunk did not differ significantly with and without tension feedback. In fact, the difference in the local minimum value of θ before/after perturbation ($\Delta\theta_{min}$) is almost the same as that without tension feedback. From Table II, there is no significant difference in $\Delta\theta_{min}$ with and without tension feedback.

From our simple model analysis, we could suspect that tension feedback suppressed the perturbation causing tilting forward but did not suppress the perturbation causing tilting backward effectively. Our quadruped model tends to tilt forward because the COG is shifted forward. Hence, the suppression of over-tilting forward owing to tension feedback improves locomotion capability, for example, preventing stumbling. On the other hand, the quadruped model does not tend to tilt backward due to the COG location. Unless the fore leg steps on the high obstacle and the robot flips backward, the perturbation causing tiling backward of the trunk can not significantly affect the robot's locomotion.

IV. Robot Design

A. Mechanical Design

We developed the musculoskeletal quadruped robot to validate our controller focusing on the phase relationship between the fore and hind legs (Fig. 1). This robot has one fore leg whose length is 0.60 [m] and one hind leg whose length is 0.76 [m]. The fore leg has the shoulder, elbow, and wrist joints, and the hind leg has the hip, knee, and ankle joints. The size of the robot (length $\times$ hight $\times$ width) is 1.20 $\times$ 0.76 $\times$ 0.05 [m], and the weight of the robot is 6.3 [kg].

6 McKibben-type PAMs [7] are arranged in the fore and hind leg, respectively (Fig. 6). In the fore leg, shoulder extensor (SE) and shoulder flexor (SF) drive the shoulder joint, elbow extensor (EE) drives the elbow joint, wrist flexor (WF) drives the wrist joint, Lastissimus Dorsi (LD) drives the shouder and elbow joints, and Triceps Brachii (TB) drives the elbow and wrist joints. In the hind leg, hip extensor (HE) and hip flexor (HF) drive the hip joint, knee extensor (KE) drives the knee joint, ankle flexor (AF) drives the ankle joint, Semimembranosus (SM) drives the hip and knee joints, and Gastrocnemius (GA) drives the knee and ankle joints.

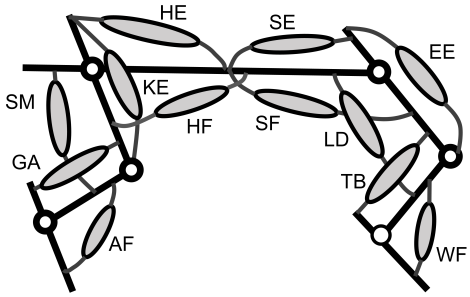

Fig. 6: Muscle arrangement of quadruped robot.

12 on-off solenoid valves (VQZ1321-6L1-C6, SMC) supply and exhaust compressed air (0.4 [MPa]) for PAMs. A control board (Arduino Due) sends the control signal to these valves.

B. Tension Sensor Design

To stably measure muscle tension even when the robot running over challenging terrain, we developed a durable tension sensor. Figure 7 shows an overview of the tension sensor. This tension sensor is composed of an aluminum plate, a rubber cylinder (Hanenaito GP-35LE, Naigaigomu) whose shore hardness is A33, a sensor board where a coil pattern is printed, and a 3D-printed cover. With this sensor structure, the sensor estimates tension based on the coil inductance changing [12]. When the tension is applied to both ends of the sensor, the rubber cylinder is deformed, and the aluminum plate approaches the sensor board (Fig. 8). Here, the inductance of the coil pattern decreases due to the eddy current effect. Therefore, tension can be estimated by measuring the inductance of the coil pattern. We used the first-order approximation to calculate tension from the inductance.

To measure the inductance, we used an inductance digital converter (LDC1614, Texas Instruments). Note that, the durable coil pattern is placed on the board where the pressure is applied, and the other fragile electronic components are placed on the board where the pressure is not applied. Thus, the tension sensor structure is hard to break. The size of the tension sensor (width $\times$ height $\times$ depth) is 35.0 $\times$ 37.8 $\times$ 33.0 [mm], and the weight of the tension sensor is 25.3 [g].

C. Control

To calculate our nonlinear oscillator every 15 [ms], as Eqs. (1) and (2), in the developed robot, we define $T_F = T_{TB}$ and $T_H = T_{GA}$, where T_{TB} and T_{GA} are tension of TB and GA. T_{TB} and T_{GA} change significantly when the fore or hind legs contact with the ground because TB and GA are the extensor muscles arranged at the distal end of the leg. Hence, we can detect the environment changing delicately through T_{TB} and T_{GA}.

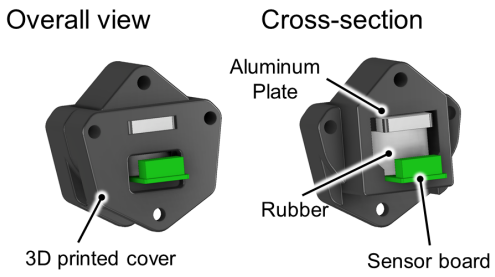

Fig. 7: Tension sensor structure.

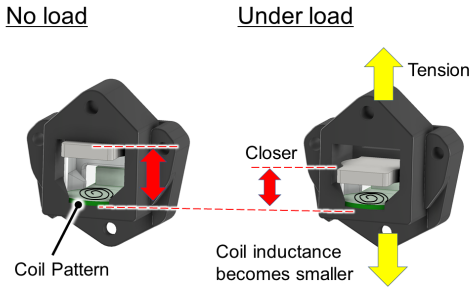

Fig. 8: Tension sensor mechanism.

We designed a muscle activation pattern based on the phase ϕ_i. ϕ_i is divided into four phases, and muscle activation patterns are assigned in each phase as shown in Fig. 9. The control board opens the solenoid valves connecting to the muscles shown in Fig. 9 and closes the solenoid valves connecting to the muscles not shown in Fig. 9. Here, if the parameters to divide ϕ_i are α_i, β_i $(i = F, H)$, the muscle activation pattern is designed as follows: (i) $0 \leq \phi_i < \pi\alpha_i$ is the swing phase when the leg is lifted forward, (ii) $\pi\alpha_i \leq \phi_i < \pi$ is the touch down phase when the leg is extended forward, (iii) $\pi \leq \phi_i < 2\pi\beta_i$ is the early stance phase when the leg is extended backward, (iv) $2\pi\beta_i \leq \phi_i < 2\pi$ is the late stance phase when the leg is more extended backward than the early stance phase. Note that this pattern satisfies the design requirement for the non-linear oscillator that each leg should generate pushing-off force for $\pi \leq \phi_i < 2\pi$.

V. Experimental Setup

The developed quadruped robot doesn't have right and left legs and can not balance right and left. Hence, the robot's locomotion is constrained with the boom (length: 1.5[m]) as shown in Fig. 10. The robot has 3 degrees of freedom (DOF): 2 DOF to move in the x and y directions and 1 DOF to rotate in the θ direction. Owing to this constraint, the robot's position and velocity are measured from the boom angle. θ and the boom angle is measured with IMU (Inertial Measurement Unit) (BNO055, BOSCH).

We set the flat and uneven terrain to verify the effectiveness of our proposed controller. On the flat terrain, no obstacle was set around the pole. The distance of the flat

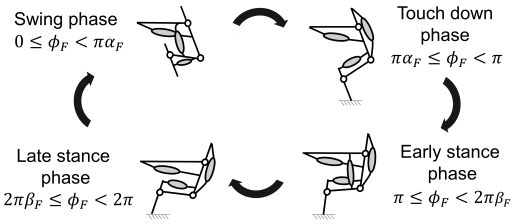

(a) Muscle activation pattern for fore leg.

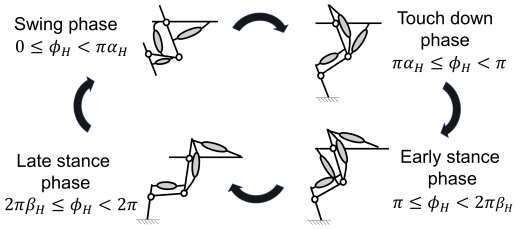

(b) Muscle activation pattern for hind leg.

Fig. 9: Muscle activation pattern ((a) fore leg, (b) hind leg).

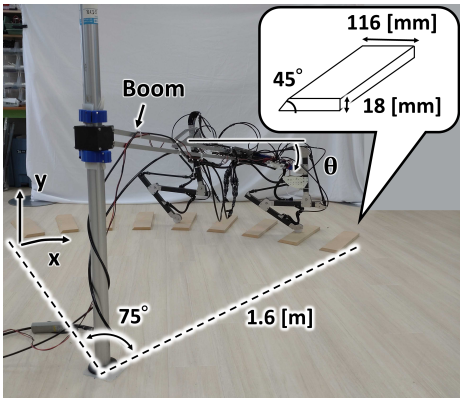

Fig. 10: Experimental setup.

terrain is an arc with a radius of 1.6 [m] and an angle of 180 [deg]. Conversely, on the uneven terrain, 9 obstacles are set around the pole. The distance of the uneven terrain is an arc with a radius of 1.6 [m] and an angle of 75.0 [deg]. Under uneven terrain conditions, the robot starts to run 2 or 3 steps before the obstacles, continues running over the obstacles, and stops running after crossing the obstacles.

The control parameters of the non-linear oscillator and muscle are set as shown in Table III. Before the experiment, these parameters are decided such that the robot could walk flat terrain with $(\sigma_F, \sigma_H \neq 0)$ and without $(\sigma_F, \sigma_H = 0)$ tension feedback.

VI. Results and Discussion

In the running experiment, similar to the numerical simulation, the effectiveness of the proposed controller was also validated by comparing the cases with and without tension feedback. Before conducting an experiment over uneven ter-

TABLE III: Control parameters

Parameter	Value
ω	10.54 [rad/s]
ϵ_F, ϵ_H	1.0
$\Delta\phi$	$\pi/3$ [rad]
α_F	0.8
α_H	0.8
β_F	0.667
β_H	0.667

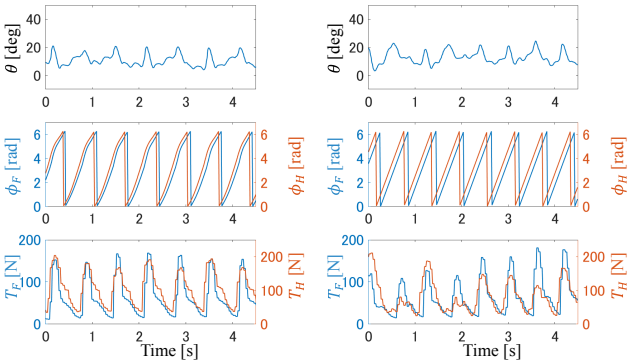

(a) With tension feedback (b) Without tension feedback

Fig. 11: Experimental results over flat terrain with $(\sigma_F, \sigma_H) = (0.6, 0.4)$ and without $(\sigma_F, \sigma_H) = (0, 0)$ tension feedback. Phase (ϕ_F, ϕ_H), trunk posture angle (θ), and tension (T_F, T_H) are shown.

rain, we carried out an experiment over flat terrain to measure the baseline behavior of the robot's locomotion. Figure. 11 shows the phase (ϕ_F, ϕ_H), the trunk posture angle (θ), and the tension (T_F, T_H) with and without tension feedback over flat terrain. While ϕ_i and T_j oscillated differently, θ oscillated with similar amplitudes with and without tension feedback. These results show that over flat terrain, the trunk posture behavior did not differ whether tension feedback was applied or not.

Next, we conducted an experiment over uneven terrain to validate that our CPG-based controller could stabilize the robot's locomotion. Figure. 12 shows the phase (ϕ_F, ϕ_H), the trunk posture angle (θ), and the tension (T_F, T_H) with and without tension feedback over uneven terrain. We observed that at $t = 3.0$ [s] with tension feedback, the trunk tilted forward, and T_F was higher than T_H (Fig. 12(a)). Furthermore, ϕ_F was delayed, and ϕ_F and ϕ_H were aligned, which was also observed in the numerical simulation (Fig. 4(a)). Consequently, the oscillation of θ did not increase significantly after $t = 3.0$ [s].

It is apparent that both with and without tension feedback, the oscillation of θ over uneven terrain was more significant than that over flat terrain. To quantify how much the oscillation of θ increased by changing the terrain from flat to uneven, we plotted the maximum and minimum values of θ for each trial (Fig. 13). Both with and without tension feedback, θ_{min} decreased by a similar amount when the terrain changed from flat to uneven. Conversely, the increase

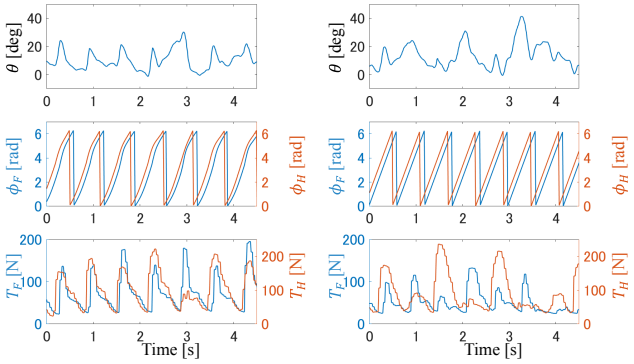

(a) With tension feedback (b) Without tension feedback

Fig. 12: Experimental results over uneven terrain with $(\sigma_F, \sigma_H) = (0.6, 0.4)$ and without $(\sigma_F, \sigma_H) = (0, 0)$ tension feedback. Phase (ϕ_F, ϕ_H), trunk posture angle (θ), and tension (T_F, T_H) are shown.

of θ_{max} with tension feedback was lower than that without tension feedback. These results show that tension feedback suppressed the oscillation of θ by preventing the trunk from tilting forward.

Finally, we investigated the impact of the stabilized trunk posture on running velocity. Figure 14 shows the running velocity with and without tension feedback. With tension feedback, the velocity decreased by 18.8% when the terrain changed from flat to uneven. In contrast, without tension feedback, the velocity decreased by 46.4% when the terrain changed from flat to uneven. The stable trunk posture brought about by tension feedback prevented stumbling and velocity reduction.

VII. Conclusion

In this paper, we proposed tension feedback control for a musculoskeletal quadruped robot driven by PAMs. To develop the control, we solved two problems as described in the introduction. First, we proposed a non-linear oscillator that calculates the phase of the gait based on the muscle tension. This control architecture does not need precise control like model-based control, which is suitable for PAMs-driven robots. Second, we developed a new tension sensor measuring muscle tension as proprioceptive information. This sensor is very durable because the force is not applied to the fragile electronic components. By using this sensor, our robot could measure tension and modulate the phase of the gait to adapt to uneven terrain.

We have shown several simulations and experimental results to show tension feedback stabilized the robot's locomotion. However, our simulation model and robot have only two legs, which indicates that to bring the robot into more challenging environments, the robot must use two additional legs and support its body. In the near future, it is essential to extend our proposed controller to investigate how to use four legs adaptively.

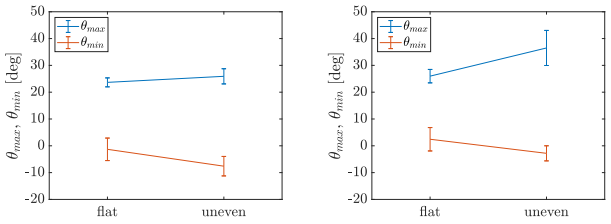

(a) With tension feedback (b) Without tension feedback

Fig. 13: Maximum and minimum values of θ over flat and uneven terrain: (a) with tension feedback $(\sigma_F, \sigma_H) = (0.6, 0.4)$ and (b) without tension feedback $(\sigma_F, \sigma_H) = (0, 0)$. θ_{max} is maximum value of θ, and θ_{min} is minimum value of θ for each trial. Each mean value and standard deviation were calculated using 10 data sets.

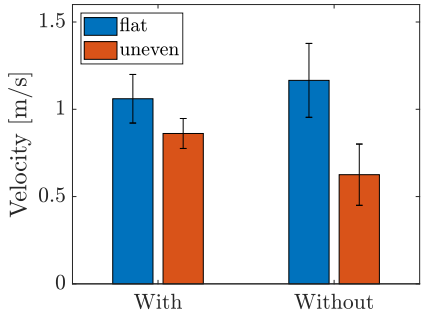

Fig. 14: Running velocity with $(\sigma_F, \sigma_H) = (0.6, 0.4)$ and without $(\sigma_F, \sigma_H) = (0, 0)$ tension feedback. Blue bar shows velocity over flat terrain, and orange bar shows velocity over uneven terrain. Each mean value and standard deviation were calculated using 10 data sets.

REFERENCES

[1] M. Hutter, C. Gehring, D. Jud, A. Lauber, C. D. Bellicoso, V. Tsounis, J. Hwangbo, K. Bodie, P. Fankhauser, M. Bloesch, *et al.*, "Anymal-a highly mobile and dynamic quadrupedal robot," in *2016 IEEE/RSJ international conference on intelligent robots and systems (IROS)*, pp. 38–44, IEEE, 2016.

[2] B. Katz, J. Di Carlo, and S. Kim, "Mini cheetah: A platform for pushing the limits of dynamic quadruped control," in *2019 IEEE international conference on robotics and automation (ICRA)*, pp. 6295–6301, IEEE, 2019.

[3] C. Gehring, S. Coros, M. Hutter, M. Bloesch, M. A. Hoepflinger, and R. Siegwart, "Control of dynamic gaits for a quadrupedal robot," in *2013 IEEE international conference on Robotics and automation (ICRA)*, pp. 3287–3292, IEEE, 2013.

[4] J. Hwangbo, J. Lee, A. Dosovitskiy, D. Bellicoso, V. Tsounis, V. Koltun, and M. Hutter, "Learning agile and dynamic motor skills for legged robots," *Science Robotics*, vol. 4, no. 26, p. eaau5872, 2019.

[5] J. Lee, J. Hwangbo, L. Wellhausen, V. Koltun, and M. Hutter, "Learning quadrupedal locomotion over challenging terrain," *Science robotics*, vol. 5, no. 47, p. eabc5986, 2020.

[6] G. A. Pratt and M. M. Williamson, "Series elastic actuators," in *1995 IEEE/RSJ International Conference on Intelligent Robots and Systems (IROS)*, vol. 1, pp. 399–406, IEEE, 1995.

[7] C.-P. Chou and B. Hannaford, "Measurement and modeling of mckibben pneumatic artificial muscles," *IEEE Transactions on robotics and automation*, vol. 12, no. 1, pp. 90–102, 1996.

[8] S. Nakatsu, A. Rosendo, M. Shimizu, and K. Hosoda, "Realization of three-dimensional walking of a cheetah-modeled bio-inspired quadruped robot," in *2014 IEEE international conference on robotics and biomimetics (ROBIO)*, pp. 779–784, IEEE, 2014.

[9] K. Narioka, A. Rosendo, A. Sproewitz, and K. Hosoda, "Development of a minimalistic pneumatic quadruped robot for fast locomotion," in *2012 IEEE International Conference on Robotics and Biomimetics (ROBIO)*, pp. 307–311, IEEE, 2012.

[10] H. Tanaka, T.-Y. Chen, and K. Hosoda, "Dynamic turning of a soft quadruped robot by changing phase difference," *Frontiers in Robotics and AI*, vol. 8, p. 629523, 2021.

[11] A. Rosendo, S. Nakatsu, K. Narioka, and K. Hosoda, "Producing alternating gait on uncoupled feline hindlimbs: muscular unloading rule on a biomimetic robot," *Advanced Robotics*, vol. 28, no. 6, pp. 351–365, 2014.

[12] H. Wang, D. Jones, G. de Boer, J. Kow, L. Beccai, A. Alazmani, and P. Culmer, "Design and characterization of tri-axis soft inductive tactile sensors," *IEEE Sensors Journal*, vol. 18, no. 19, pp. 7793–7801, 2018.

[13] S. Grillner, "Neurobiological bases of rhythmic motor acts in vertebrates," *Science*, vol. 228, no. 4696, pp. 143–149, 1985.

[14] H. Kimura, Y. Fukuoka, and A. H. Cohen, "Biologically inspired adaptive walking of a quadruped robot," *Philosophical Transactions of the Royal Society A: Mathematical, Physical and Engineering Sciences*, vol. 365, no. 1850, pp. 153–170, 2007.

[15] Y. Kuramoto, "Self-entrainment of a population of coupled non-linear oscillators," in *International Symposium on Mathematical Problems in Theoretical Physics*, pp. 420–422, Springer, 1975.

[16] D. Owaki, T. Kano, K. Nagasawa, A. Tero, and A. Ishiguro, "Simple robot suggests physical interlimb communication is essential for quadruped walking," *Journal of The Royal Society Interface*, vol. 10, no. 78, p. 20120669, 2013.

[17] H. Tanaka, O. Matsumoto, T. Kawasetsu, and K. Hosoda, "Swinging mass for energy-efficient quadrupedal locomotion," *Advanced Robotics*, pp. 1–10, 2023.

[18] R. Zamboni, D. Owaki, and M. Hayashibe, "Adaptive and energy-efficient optimal control in cpgs through tegotae-based feedback," *Frontiers in Robotics and AI*, vol. 8, p. 632804, 2021.